# Semiactive Backstepping Control for Vibration Reduction in a Structure with Magnetorheological Damper Subject to Seismic Motions

MAURICIO ZAPATEIRO,[1,*] HAMID REZA KARIMI,[2] NINGSU LUO,[1] BRIAN M. PHILLIPS[3] AND BILLIE F. SPENCER JR[3]

[1]*Institute of Informatics and Applications, University of Girona, Girona, Spain*

[2]*Faculty of Technology and Science, University of Agder, Grimstad, Norway*

[3]*Department of Civil and Environmental Engineering, University of Illinois at Urbana, Champaign, USA*

**ABSTRACT:** The use of magnetorheological (MR) dampers for mitigating vibrations caused by seismic motions in civil engineering structures has attracted much interest in the scientific community because of the advantages of this class of device. It is known that MR dampers can generate high damping forces with low energy requirements and low cost of production. However, the complex dynamics that characterize MR dampers make difficult the control design for achieving the vibration reduction goals in an efficient manner. In this article, a semiactive controller based on the backstepping technique is proposed. The controller was applied to a three-story building with an MR damper at its first floor subjected to seismic motions. The performance of the controller was evaluated experimentally by means of real time hybrid testing.

*Key Words:* magnetorheological damper, smart structures, vibration reduction, semiactive control.

## INTRODUCTION

THE protection of structures has always been a major concern in civil engineering, in particular when these structures are built in places prone to hazardous weather conditions (e.g., hurricanes, tsunamis), in zones of intense seismic activity, or when the structure is subjected to heavy loadings (e.g., heavy traffic on a bridge). When structures are not well protected against these phenomena, they could sustain severe damage and, as a consequence, cause personal injuries or death, as experienced in earthquakes in Mexico City (1985), Kobe (1995), northwestern Turkey (1999), or those that struck southern Asia in 2004 followed by tsunamis, or more recently in China (2008).

In a first attempt to make structures resistant to these hazardous phenomena, passive dampers were designed to alleviate the energy dissipation of the main structure by absorbing part of the input energy, thereby reducing the structural damage. These dampers do not need external power sources. However, once tuned, there is no way to make them adaptable to different loading conditions; non-linear devices such as lead-rubber bearings, friction-pendulum bearings or high damping rubber bearings are often used (Yoshioka et al., 2002).

The adaptation limitation of passive dampers can be overcome by active dampers. With active devices, it is possible to determine the forces that stabilize the structure, and the system can be adapted to changing loading conditions. Active control devices, unlike passive ones, do require external power sources, and can inject energy into the system. Additionally, sensors and controllers are required (Spencer and Sain, 1997).

Some problems of active systems are the large power requirements and the frequent lack of electrical supply, for example during an earthquake or hurricane. Moreover, these systems inject energy into the structure, and may destabilize it in a bounded-input bounded-output sense. These concerns, in addition to the limitations of passive systems with respect to varying loadings, have led to another solution: hybrid and semiactive devices, which are particularly promising in addressing a number of these problems (Dyke et al., 1998).

Semiactive control devices combine the features of active and passive devices: their properties can be adapted in real time, but they cannot inject energy into the system. Semiactive devices have been shown to perform significantly better than passive devices, and as well as active devices, without requiring large power sources, thus allowing for battery operation (Spencer and Song, 1999).

*Author to whom correspondence should be addressed.
E-mail: mauricio.zapateiro@udg.edu
Figures 1–19 appear in color online: http://jim.sagepub.com



1045-389X/09/17 2037–17 $10.00/0 DOI: 10.1177/1045389X09343024

MR fluid dampers are one of the most attractive semiactive devices. Compared to other devices of their class, MR dampers can generate a high yield strength, have low costs of production, require low power, and have a fast response and small size. The complex nonlinear behavior of the MR dampers makes mathematical characterization challenging and controller implementation difficult for vibration control. Recently, a computational algorithm was presented for the modeling and identification of MR dampers using wavelet systems to handle the non-linear terms by Karimi et al. (2009).

A number of control techniques have been developed for systems with MR dampers. The clipped optimal control (Dyke et al., 1996) was one of the first controllers developed for this class of systems. An optimal controller is designed to estimate the force that mitigates the vibrations in the structure. However, the MR damper dynamics are ignored and the control signal takes on two values only, chosen according to an algorithm.

The control based on Lyapunov's stability theory has been used and successfully tested in structures such as buildings, bridges, and car suspension systems (Jansen and Dyke, 2000; Wang and Gordaninejad, 2002; Yang et al., 2002; Luo et al., 2003; Park and Jeon, 2002; Nagarajaiah et al., 2006). The control objective was to choose control inputs in such a way as to make the derivative of the Lyapunov function as negative as possible.

Other control methods have been proposed, such as the bang-bang control (McClamroch et al., 1994; McClamroch and Gavin, 1995; Jansen and Dyke, 2000); sliding mode control (Luo et al., 2003; Moon et al., 2003; Villamizar et al., 2003); quantitative feedback theory control (Villamizar et al., 2004; Zapateiro et al., 2008); and intelligent controls such as fuzzy logic and neuro fuzzy control (Schurter and Roschke, 2001; Kim and Roschke, 2006).

Backstepping control was first proposed in systems with MR dampers by Villamizar et al. (2005) and Luo et al. (2007). Backstepping control design consists in selecting appropriate functions of state variables as pseudo control inputs for lower dimension subsystems of the overall system. Each backstepping stage is a new pseudo control design in terms of the preceding stages. The final result is a feedback design for the true control input, which achieves the original design objective by virtue of a final Lyapunov function formed by summing up the Lyapunov functions associated with each individual design stage.

Numerical simulations and experiments on small-scale specimens showed the feasibility of backstepping control implementation in larger systems. This fact was explored in this article. A backstepping controller was designed for a large-scale structure equipped with an MR damper, and experiments were run on a real-time hybrid testing (RTHT) basis to evaluate its performance.

This article is organized as follows. Section 'Backstepping Control' explains the basic concepts about backstepping control. Section 'Experimental Setup' describes the experimental environment and the structure model that was used for control design. Section 'Backstepping Controller Formulation' presents the details of the backstepping controller formulation for the experimental structure. Section 'Experimental Results' presents the experimental results and the controller performance analysis. Finally, the conclusions are outlined in section 'Conclusions'.

## BACKSTEPPING CONTROL

The general idea behind the backstepping control design is based on the following assumption (Krstic et al., 1995):

**Assumption 2.1.** *Consider the system:*

$$\dot{x} = f(x) + g(x)u, \quad f(0) = 0, \tag{1}$$

*where $x \in \mathbb{R}$ is the state and $u \in \mathbb{R}$ is the control input. There exists a continuously differentiable feedback control law $u = \alpha(x)$ with $\alpha(0) = 0$ and a smooth, positive definite, radially unbounded function $V : \mathbb{R}^n \to \mathbb{R}$, such that*

$$\frac{\partial V(x)}{\partial x}[f(x) + g(x)\alpha(x)] \leq -W(x) \leq 0, \quad \forall x \in \mathbb{R}^n, \tag{2}$$

*where $W : \mathbb{R}^n \to \mathbb{R}$ is positive semidefinite.*

Under this assumption, the control $u = \alpha(x)$ guarantees the global boundedness of $x(t)$ and via the LaSalle–Yoshizawa theorem:

$$\lim_{t \to \infty} W(x(t)) = 0 \tag{3}$$

The following lemma states the basis for the backstepping design:

**Lemma 2.1.** *Let the system of Equation (1) be augmented by an integrator:*

$$\begin{aligned} \dot{x} &= f(x) + g(x)\xi \\ \dot{\xi} &= u, \end{aligned} \tag{4}$$

*and suppose that $\dot{x}$ satisfies Assumption 1 with $\xi \in \mathbb{R}$ as its control. If $W(x)$ is positive definite, then:*

$$V_a(x,\xi) = V(x) + \frac{1}{2}[\xi - \alpha(x)]^2, \tag{5}$$

*is a control Lyapunov function for the full system of Equation (4), that is, there exists a feedback control $u = \alpha(x,\xi)$ which renders $x = 0$, $\xi = 0$ the global asymptotic stable equilibrium of Equation (1). If $W(x)$ is only positive semidefinite, then there exists a feedback control that renders $V_a \le -W_a(x,\xi) \le 0$, such that $W_a(x,\xi) > 0$ whenever $W(x) > 0$ or $\xi \ne \alpha(x)$. This guarantees global boundedness and convergence of $[x(t), \xi(t)]^T$ to the largest invariance set $M_a$ contained in the set $E_a$ $\{[x,\xi]^T \in \mathbb{R}^{n+1} | W(x) = 0, \xi = \alpha(x)\}$.*

The backstepping technique introduced in this section can easily be extended by recursion to larger order systems and more general cases.

## EXPERIMENTAL SETUP

This section describes the experimental environment where the controller was tested. Experiments were executed in an RTHT configuration available at the Smart Structures Technology Laboratory, University of Illinois Urbana, Champaign (USA), shown in Figure 1. It consists of a computer that simulates the structure to be controlled and generates the commanding signals (displacements and control signals); a small-scale MR damper that is driven by a hydraulic actuator, which in turn is controlled by a servo-hydraulic controller; and Digital Signal Processor, Analog-to-Digital (A/D) and Digital-to-Analog (D/A) hardware for signal processing. Sensors available include a linear variable displacement transformer (LVDT) for displacement measurements and a load cell for measuring the MR damper force. In Figure 1, $x_{cmd}$ is the commanded displacement, $f_{\mathrm{mr}}$ is the MR damper force measured by the load cell, $x_{\mathrm{meas}}$ is the displacement measured by the LVDT and $i$ is the control current sent to the hydraulic actuator. A fully detailed description of this RTHT implementation can be found in Carrion and Spencer (2007).

### Structure Model

The schematic of the three-story building to be controlled is shown in Figure 2. The building was modeled with the second-order motion equation:

$$\mathbf{M_s}\ddot{\mathbf{x}} + \mathbf{C_s}\dot{\mathbf{x}} + \mathbf{K_s}\mathrm{x} = G_s f - \mathbf{M_s} L_s \ddot{x}_g, \tag{6}$$

where the matrices and vectors $\mathbf{M_s}$, $\mathbf{C_s}$, $\mathbf{K_s}$, $G_s$, and $L_s$ are given by:

$$\mathbf{M_s} = \begin{bmatrix} m_1 & 0 & 0 \\ 0 & m_2 & 0 \\ 0 & 0 & m_3 \end{bmatrix} = \begin{bmatrix} 20253 & 0 & 0 \\ 0 & 20253 & 0 \\ 0 & 0 & 20253 \end{bmatrix} \mathrm{kg} \tag{7}$$

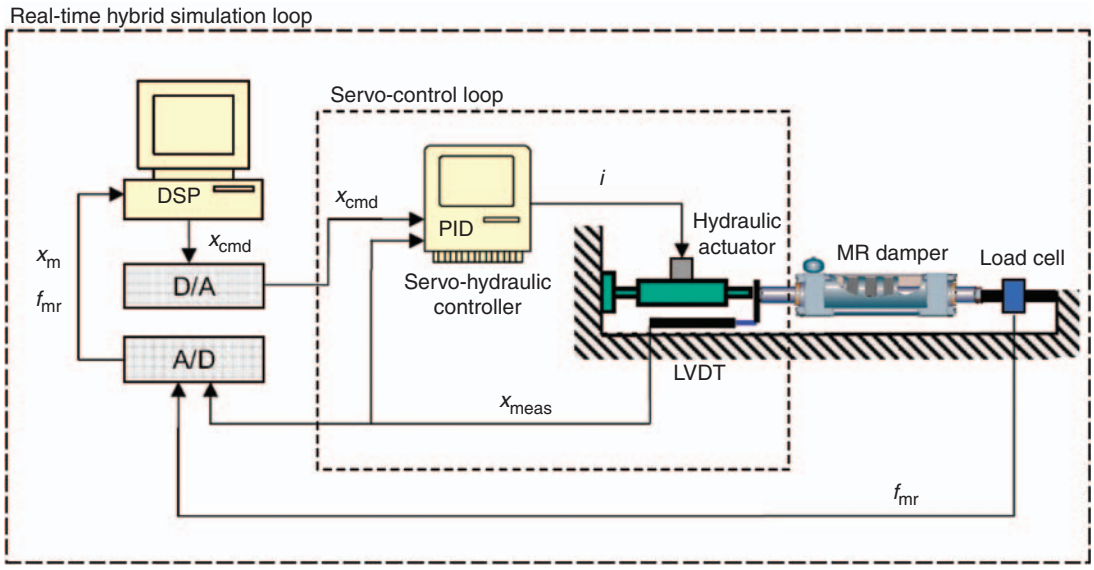


***Figure 1.*** *RTHT system schematic.*

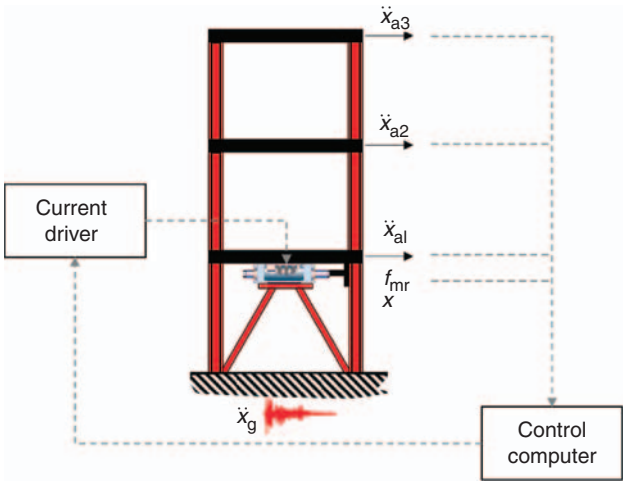


***Figure 2.*** *Schematic of the 3-story building with MR damper.*

$$\mathbf{C_s} = \begin{bmatrix} c_{11} & c_{12} & 0 \\ c_{21} & c_{22} & c_{23} \\ 0 & c_{32} & c_{33} \end{bmatrix} = \begin{bmatrix} 7243.2 & -2070 & 0 \\ -2070 & 4138.2 & -2070 \\ 0 & -2070 & 2070 \end{bmatrix} \text{N s/m} \tag{8}$$

$$\mathbf{K_s} = \begin{bmatrix} k_{11} & k_{12} & 0 \\ k_{21} & k_{22} & k_{23} \\ 0 & k_{32} & k_{33} \end{bmatrix} = \begin{bmatrix} 9932 & -5661 & 0 \\ -5661 & 11338 & -5661 \\ 0 & -5661 & 5661 \end{bmatrix} \text{N/m} \tag{9}$$

$$G_s = [-1, 0, 0]^T \quad L_s = [1, 1, 1]^T \tag{10}$$

$\mathbf{x}$ is the vector of relative displacements, i.e., with respect to the ground; $f$ is the MR damper force and $\ddot{x}_g$ is the incoming earthquake acceleration. $x_{ai}$ is the absolute acceleration of the $i$-th floor. The absolute displacement is measured with respect to an inertial frame, so the relationship between relative and absolute coordinates is: $x = x_a - x_g$. The natural frequencies and the damping ratios of the structure corresponding to the first, second, and third mode were 1.09 Hz (0.31%), 3.17 Hz (0.62%), and 4.74 Hz (0.63%), respectively.

## MR Damper

The MR damper used in the experiments was the RD-1005 manufactured by the Lord Corporation (Cary, NC, USA – www.lord.com), shown in Figure 3. The damper was 216 mm long in its extended position, 38.1 mm in diameter and had a stroke of 25.4 mm. It contained 50 mL of MR fluid and could generate

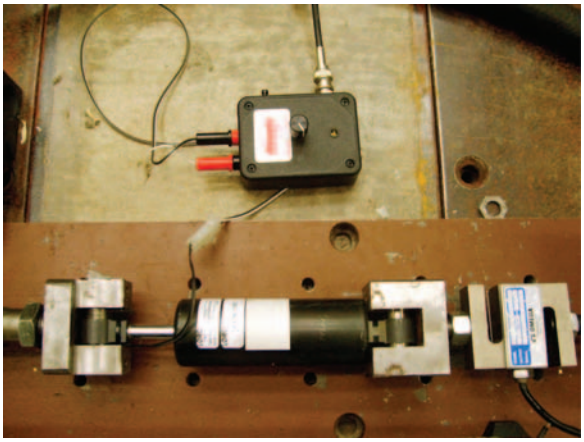

***Figure 3.*** *MR damper and PWM system.*

forces up to 3000 N. The magnetic field was generated by the current from a PWM amplifier (the RD-1002 Wonder Box, from Lord Corp.).

The dynamics of the damper can be modeled by the Bouc–Wen model (Spencer et al., 1997), as shown in Equations (11)–(12):

$$f_{\text{mr}} = (c_{0a} + c_{0b}u)\dot{x}_{1r} + (k_{0a} + k_{0b}u)x_{1r} + (\alpha_a + \alpha_b u)z \tag{11}$$

$$\dot{z} = -\gamma|\dot{x}_{1r}|z|z|^{n-1} - \beta\dot{x}_{1r}|z|^n + A\dot{x}_{1r}, \tag{12}$$

where $f_{\text{mr}}$ is the damper force, $x_{1r}$ is the piston displacement, $c_0 = c_{0a} + c_{0b}u$ is the damping coefficient (voltage dependent) and $k_0 = k_{0a} + k_{0b}u$ is the damper stiffness (voltage dependent); $z$ is an evolutionary variable that describes the hysteretic behavior of the damper; $A$, $\gamma$, $\beta$, and $n$ are design parameters that can be adjusted to fit the hysteretic response of the damper; $u$ is the output of the first-order filter introduced to account for the time that the MR fluid takes to reach rheological equilibrium:

$$\dot{u} = -\eta(u - v) \tag{13}$$

where $\eta$ is a parameter obtained experimentally. The parameters of the MR damper were fitted using non-linear least squares parameter estimation to fit the experimental response of the damper. The damper was subject to sinusoidal and random displacements and varying voltages between 0 and 5 V. As a result, the parameters obtained were: $\alpha_a = 33.27$ N/m, $\alpha_b = 182.65$ N/m V, $c_{0a} = 754.41$ N s/m, $c_{0b} = 712.73$ N s/m V, $k_{0a} = 1137.57$ N/m, $k_{0b} = 1443.50$ N/m V, $x_0 = 0$ m, $\gamma = 4209.8\,\text{m}^{-2}$, $\beta = 4205.2\,\text{m}^{-2}$, $A = 10246$, $n = 2$, $\eta = 57\,\text{s}^{-1}$. The following scaling factors were used to

integrate the physical small-scale MR damper to the numerical large-scale structure: the first floor relative displacement was reduced by a factor $S_L = 7.25$ to obtain the damper piston displacement and the MR damper force was increased by a factor $S_F = 60$ to obtain the input force on the structure.

Figures 4 and 5 show a comparison between the experimental dynamics of the MR damper and that

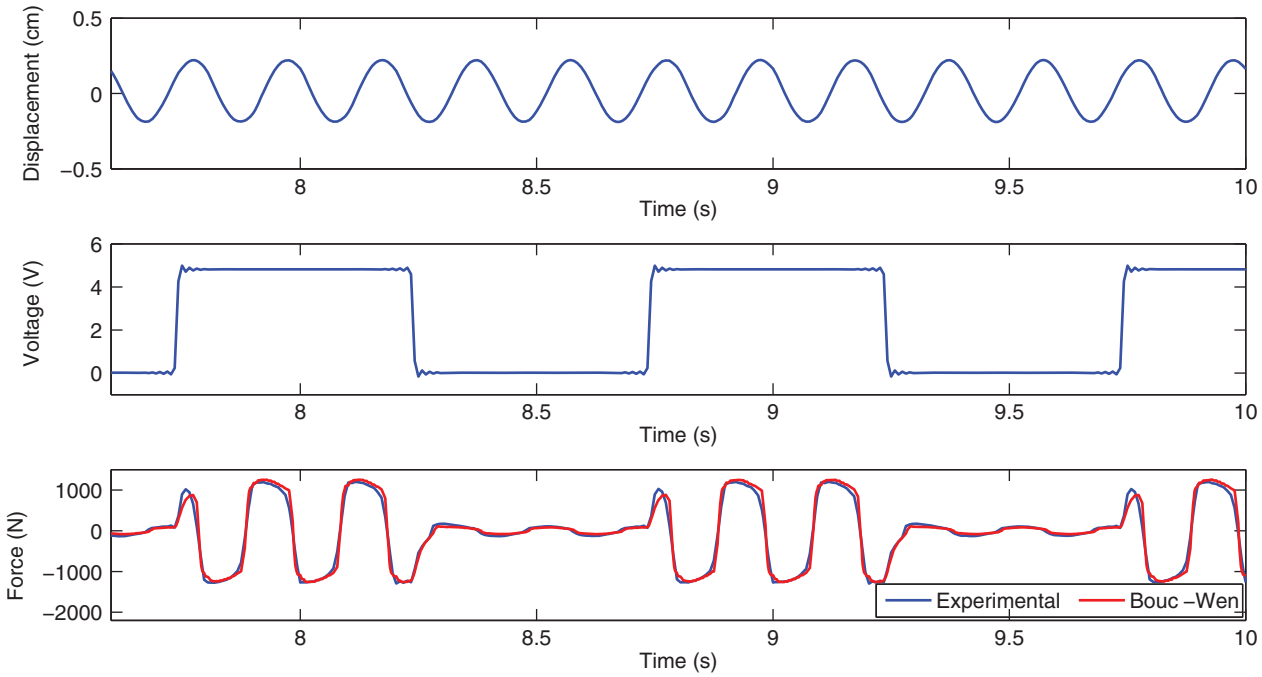


***Figure 4.*** *Time behavior of the MR damper characteristics: sinusoidal displacement and switching voltage.*

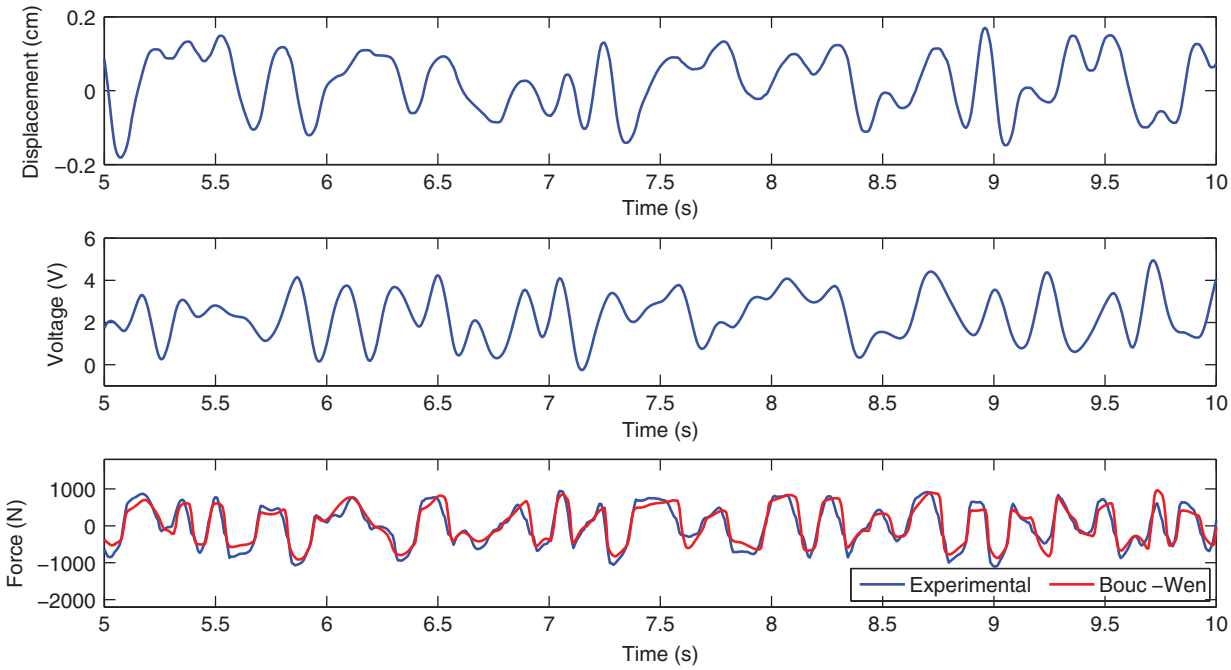


***Figure 5.*** *Time behavior of the MR damper characteristics: random displacement and voltage.*

predicted by the Bouc–Wen model (Equations (11) and (12)) after parameter estimation. In the first case, the damper was subject to sinusoidal displacement at 5 Hz and 0.254 cm amplitude. The voltage periodically switches between 0 and 5 V. The force, measured by the load cell, was recorded and compared to that in the model. In the second case, a similar experiment was carried out, but the damper was subject to random displacement and random voltage excitations.

### Hydraulic Actuator Dynamics

The MR damper was driven by a hydraulic actuator that received its command signal to impose a displacement from the computer running the simulation. A block diagram showing the interaction between the numerical model and the dynamic system is illustrated in Figure 6.

The entire physical system can be modeled by a transfer function $G_{xu}(s)$, whose input $u_c$ is the commanded displacement and output $x$ is the piston displacement. Modeling the dynamic systems was useful for simulating the RTHT experiments. The transfer function $G_{xu}(s)$ varied according to the input voltage of the MR damper. Two cases were identified corresponding to the damper operating at $V_0 = 0\,\text{V}$ ($G_{xu,\,V_0}(s)$) and $V_{\max} = 5\,\text{V}$ ($G_{xu,\,V_{\max}}(s)$), respectively. These transfer functions are given by:

$$G_{xu,\,V_0}(s) = \frac{1}{(0.0062s+1)(2.639\times10^{-5}s^2+0.059s+1)} \tag{14}$$

$$G_{xu,\,V_{\max}}(s) = \frac{1}{(0.0094s+1)(2.618\times10^{-5}s^2+0.058s+1)} \tag{15}$$

A bumpless transfer algorithm was developed by Carrion and Spencer (2007) to provide a smooth transition from $G_{xu,V_0}(s)$ to $G_{xu,V_{\max}}(s)$ and vice versa when the damper voltage varies during the experiments. A block diagram of this algorithm is shown in Figure 7. The Laplace transform of the model is described by:

$$X(s) = X_a(s) + X_b(s)W(s) \tag{16}$$

$$X_a(s) = G_a(s)U_c(s) = G_{xu,V_0}(s)U_c(s) \tag{17}$$

$$X_b(s) = G_b(s)U_c(s) = \left(G_{xu,V_{\max}}(s) - G_{xu,V_0}(s)\right)U_c(s) \tag{18}$$

$$W(s) = G_t(s)V(s), \tag{19}$$

where $G_t(s)$ is used to model the dynamics of the actuator associated with the change in the voltage of the MR damper, providing a smooth transition between $G_a(s)$ and $G_b(s)$, and is given by:

$$G_t(s) = \frac{1/V_{\max}}{\tau_t s + 1} \tag{20}$$

where $1/V_{\max} = 0.2$ and $\tau_t = 0.0048s$ is the transition filter time constant. As the time constant becomes smaller, the transition becomes faster, approaching a simple switching algorithm, while for large values of the time constant the transition is slower and smoother.

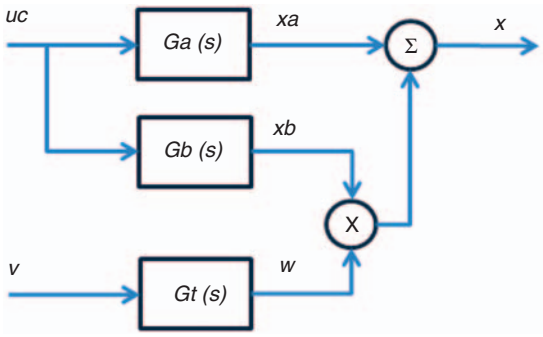


***Figure 7.*** *Block scheme of the actuator dynamics with bumpless transfer.*

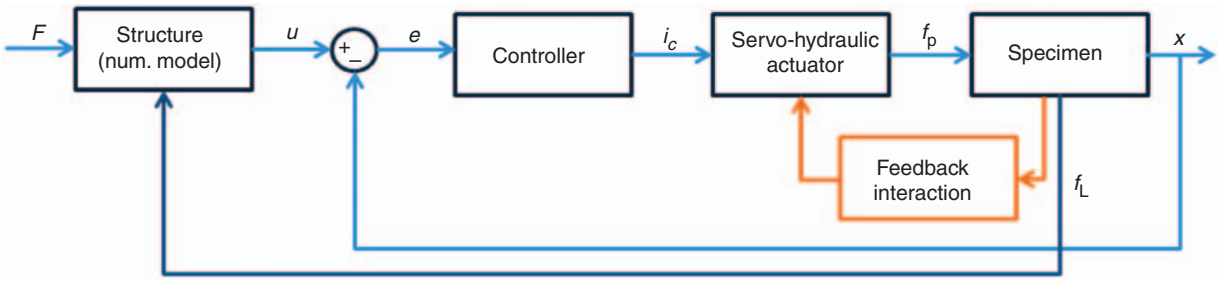


***Figure 6.*** *Numerical model and physical system interaction.*

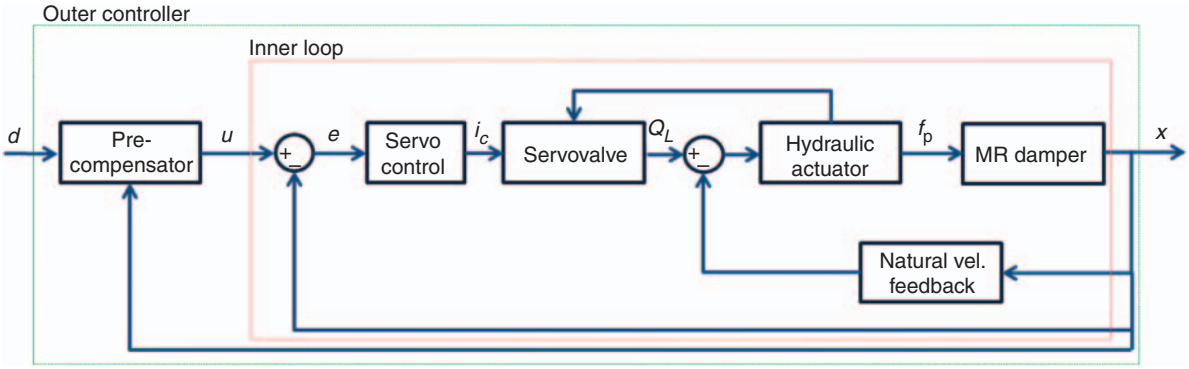


***Figure 8.*** *Diagram of the complete system with dynamics compensation.*

The output of the bumpless transfer can be written as $X(s) = G_{xu,V_0}(s)U_c(s) + (G_{xu,V_{\max}}(s) - G_{xu,V_0}(s))U_c(s)$ $G_t(s)V(s)$. It can be seen that the action of either transfer function is smoothly canceled by the filter until the desired one remains active after the transition. Because of the inherent dynamics of the physical system (e.g., time delays), a pre-compensator $G_{ff}(s)$ was added to the system for compensation purposes. In this way, the commanded displacement ($u_c$, input to the physical system) was calculated based on the desired displacement ($d$, output from the simulations) and the inverse dynamics of the physical system; as a result, $x \approx d$. A schematic of the compensated system is shown in Figure 8.

Once again, two compensators were designed: one for the MR damper operating at $V_0 = 0\,\text{V}$ ($G_{ff,V_0}(s)$) and the other for the damper operating at $V_{\max} = 5\,\text{V}$ ($G_{ff,V_{\max}}(s)$). The transfer functions are given by:

$$G_{ff,V_0}(s) = \frac{(0.062s+1)(2.639\times10^{-5}s^2+0.059s+1)}{(4.129\times10^{-4}s+1)(1.173\times10^{-7}s^2+3.909\times10^{-4}s+1)} \quad (21)$$

$$G_{ff,V_{\max}}(s) = \frac{(0.0094s+1)(2.618\times10^{-5}s^2+0.058s+1)}{(6.289\times10^{-4}s+1)(1.164\times10^{-7}s^2+3.857\times10^{-4}s+1)} \quad (22)$$

A similar approach to that of Figure 7 was followed to provide a smooth transition between both compensators. The block diagram is shown in Figure 9 and the model is described by:

$$U_{ff}(s) = U_a(s) + U_b(s)W(s) \quad (23)$$

$$U_a(s) = G_{ff,a}(s)D(s) = G_{ff,V_0}(s)D(s) \quad (24)$$

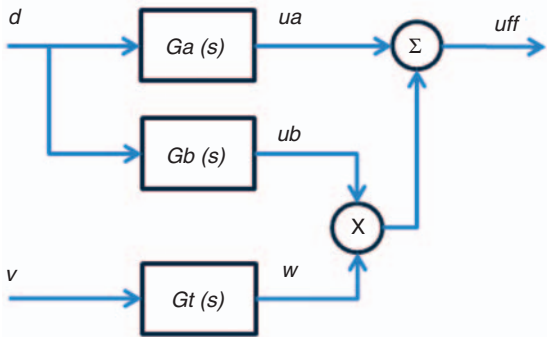


***Figure 9.*** *Block scheme of the pre-compensator dynamics with bumpless transfer.*

$$U_b(s) = G_{ff,b}(s)D(s) = \left(G_{ff,V_{\max}}(s) - G_{ff,V_0}(s)\right)D(s) \quad (25)$$

$$W(s) = G_t(s)V(s), \quad (26)$$

where $G_t(s)$ is used to provide a smooth transition between both compensators:

$$G_t(s) = \frac{0.2}{0.0048s+1} \quad (27)$$

Figure 10 shows a comparison between the desired, commanded, and measured piston displacement during the execution of an experiment where a good match between the desired and measured displacement was observed. The lower curve is a close-up of the upper one.

In order to see the performance of the system model discussed in this section, simulations were run to compare such models with the experimental response. In Figure 11 the MR damper piston displacement as measured during an experiment is compared with that obtained by the model of the overall system. That is, the system of Figure 8 was implemented in Simulink and the simulation results were compared with the experimental response. To make this comparison, the El Centro

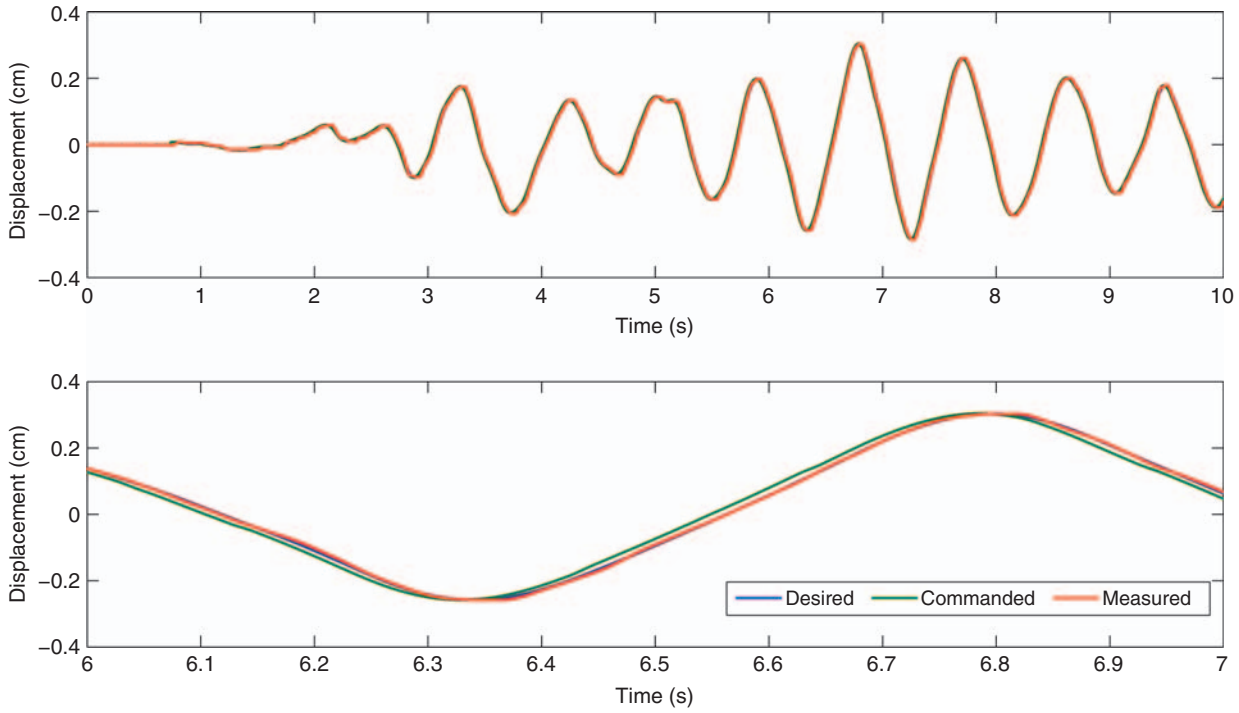


***Figure 10.*** *Comparison between the desired, commanded, and measured piston displacement.*

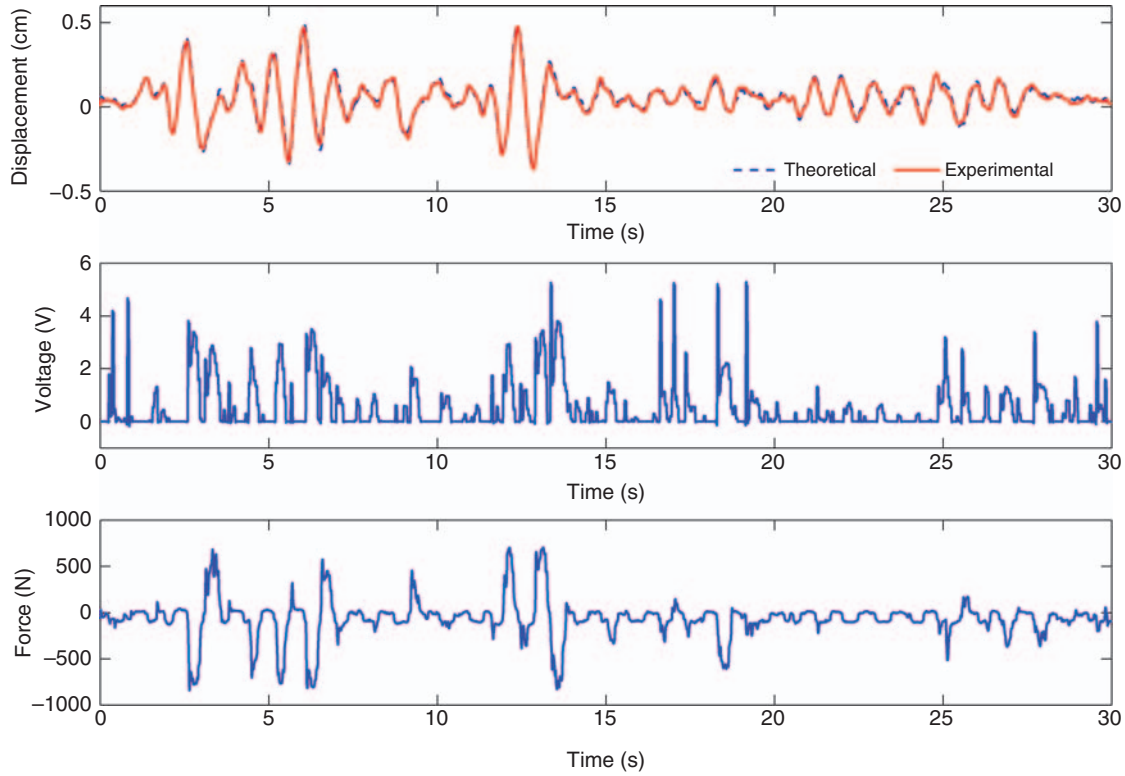


***Figure 11.*** *Comparison between the experimental and the model displacement response of the RTHT system.*

seismic motion records and MR damper voltage were taken as inputs to the RTHT system. The results show good accuracy of the system model.

## BACKSTEPPING CONTROLLER FORMULATION

To begin with the design of the backstepping controller, the structure model of Equation (6) was divided into two subsystems accounting for the first-floor dynamics, where the MR damper was attached, and the rest of the structure that accounts for the dynamics of all the floors above the base. Thus, the building can be modeled by the following set of equations:

$$S_m: \mathbf{M_{s2}}\ddot{\mathbf{x}}_{\mathbf{23a}} + \mathbf{C_{2a}}\dot{\mathbf{x}}_{\mathbf{23a}} + \mathbf{K_{s2}}\mathbf{x_{23a}} = \mathbf{B_{s2}}x_{1a} + \mathbf{F_g} \quad (28)$$

$$S_b: m_1\ddot{x}_{1a} + c_{11}\dot{x}_{1a} + k_{11}x_{1a} = -f_{\mathrm{mr}} - f_c + f_g, \quad (29)$$

where $S_m$ stands for the main structure subsystem (the two upper floors) and $S_b$ is the first floor subsystem. The $a$ sub-index means absolute coordinates; $\mathbf{x_{23a}} = [x_{2a}, x_{3a}]^T$ is the absolute acceleration vector of the two upper floors and $x_{1a}$ is the absolute acceleration of the first floor. $\mathbf{F_g} = [(c_{21} + c_{22} + c_{23})\dot{x}_g + (k_{21} + k_{22} + k_{23})x_g, 0]^T \approx [0, 0]^T$. The matrices $\mathbf{M_{s2}}$, $\mathbf{C_{s2}}$, $\mathbf{K_{s2}}$, and $\mathbf{B_{s2}}$ are given by:

$$\mathbf{M_{s2}} = \begin{bmatrix} m_2 & 0 \\ 0 & m_3 \end{bmatrix} \quad \mathbf{C_{s2}} = \begin{bmatrix} c_{22} & c_{23} \\ c_{32} & c_{33} \end{bmatrix}$$
$$\mathbf{K_{s2}} = \begin{bmatrix} k_{22} & k_{23} \\ k_{32} & k_{33} \end{bmatrix} \quad \mathbf{B_{s2}} = \begin{bmatrix} -k_{21} & -c_{21} \\ 0 & 0 \end{bmatrix} \quad (30)$$

where $f_c$ is the coupling force between the base and the main structure and $f_g$ is the force due to seismic motion:

$$f_c = c_{12}\dot{x}_{2a} + k_{12}x_{2a} \quad (31)$$

$$f_g = (c_{11} + c_{12})\dot{x}_g + (k_{11} + k_{12})x_g \quad (32)$$

The following assumptions about the intrinsic stability of the structure were used in formulating some control laws (Luo et al., 2000):

**Assumption 1.** *The unforced main structure subsystem $S_m$ is globally exponentially stable for any bounded initial conditions.*

**Assumption 2.** *If the coordinates $(x, \dot{x})$ of the base and the coupling term $\mathbf{B_{s2}}x_{1a}$ are uniformly bounded, then the main structure subsystem is stable and the coordinates $(x, \dot{x})$ of the main structure are uniformly bounded for all $t \geq 0$ and any bounded initial conditions.*

In this way, the controller was designed for the first-floor subsystem assuming that it would stabilize the overall system. Finally, to proceed with the controller formulation, Equation (29) was written in state space form, so that the backstepping technique could be applied:

$$\dot{y}_1 = y_2 \quad (33)$$

$$\dot{y}_2 = -\frac{k_{11}}{m_1}y_1 - \frac{c_{11}}{m_1}y_2 - \frac{1}{m_1}(f_{\mathrm{mr}} + f_c - f_g), \quad (34)$$

where $y_1 = x_{1a}$ and $y_2 = \dot{x}_{1a}$ are the absolute displacement and absolute velocity of the first floor. Now, we could make use of Lemma 2.1 introduced in section 'Backstepping Control' to design the backstepping controller for the more general form of Equations (33) and (34).

Consider the system of Equations (33) and (34). The following control law attenuates the vibrations and stabilizes the main structure:

$$f_{\mathrm{mr}} = (m_1 - k_{11} + h_1h_2m_1)\,y_1 + (h_1m_1 - c_{11} + h_2m_1)\,y_2 - f_c + f_g, \quad (35)$$

where $h_1$ and $h_2$ are positive constants. To demonstrate it, consider the following standard backstepping variables:

$$e_1 = y_1 \quad e_2 = y_2 - \alpha_1 \quad \alpha_1 = -h_1e_1 \quad (36)$$

Now consider the following Lyapunov function candidate and its derivative:

$$V = \frac{1}{2}e_1^2 + \frac{1}{2}e_2^2 \quad (37)$$

$$\dot{V} = e_1\dot{e}_1 + e_2\dot{e}_2 \quad (38)$$

Substitution of Equations (33), (34), and (36) into Equation (38) yields:

$$\begin{aligned}\dot{V} &= e_1\dot{e}_1 + e_2\dot{e}_2 \\ &= e_1y_1 + e_2(\dot{y}_2 - \dot{\alpha}_1) = e_1y_1 + e_2\dot{y}_2 + h_1\dot{e}_1 \\ &= e_1y_1 + e_2\left[-\frac{k_{11}}{m_1}y_1 - \frac{c_{11}}{m_1}y_2 - \frac{1}{m_1}(f_{\mathrm{mr}} + f_c - f_g)\right] \\ &\quad + h_1y_2 \end{aligned} \quad (39)$$

Substitution of Equation (35) into Equation (39) yields:

$$\dot{V} = -h_1e_1^2 - h_2e_2^2 < 0 \quad (40)$$

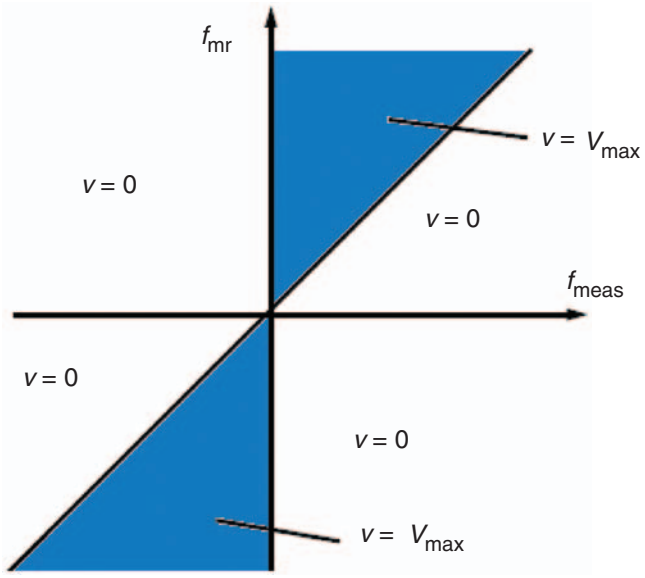


***Figure 12.*** *Graphical representation of the clipped optimal algorithm.*

According to Lyapunov's stability theory, $e_1 \to 0$ and $e_2 \to 0$. Consequently, $y = y_1 = e_1 \to 0$ and $\dot{y} = y_2 = e_2 + h_1 e_1 \to 0$. According to Assumptions 1 and 2, the vibration of the base is asymptotically attenuated and the asymptotic stability of the main structure is guaranteed.

The control law of Equation (35) cannot be implemented directly because the force to the MR damper cannot be commanded. Instead, a voltage signal had to be sent to the damper to approximately generate the desired force. Two approaches were then considered for determining the MR damper voltage that could produce the damping force required to mitigate the vibrations.

The first approach was based on the Clipped Optimal Control algorithm by Dyke et al. (1996). The algorithm is graphically depicted in Figure 12. The dynamics of the MR damper are ignored and the control signal (i.e., the voltage) takes only two values, 0 V and 5 V, according to the following algorithm:

$$u = V_{\max} H\{(f_{\text{mr}} - f_{\text{meas}}) f_{\text{meas}}\}, \tag{41}$$

where $H\{\cdot\}$ is the Heaviside function, $f_{\text{mr}}$ is the force generated by the backstepping controller and $f_{\text{meas}}$ is the actual damping force actuating on the system.

The second approach consisted of using the Bouc–Wen model of the MR damper so that its nonlinear dynamics were included in the controller design. Substituting the model of Equation (11) and solving for $u$, the following control law is obtained:

$$u = \frac{(m_1 - k_{11} + h_1 h_2 m_1) y_1 + (h_1 m_1 - c_{11} + h_2 m_1) y_2}{S_F\left[c_{0b} \frac{\dot{x}_{1r}}{S_L} + k_{0b} \frac{x_{1r}}{S_L} + \alpha_b z\right]} - \frac{+f_c - f_g + S_F\left[c_{0a} \frac{\dot{x}_{1r}}{S_L} + k_{0a} \frac{x_{1r}}{S_L} + \alpha_a z\right]}{S_F\left[c_{0b} \frac{\dot{x}_{1r}}{S_L} + k_{0b} \frac{x_{1r}}{S_L} + \alpha_b z\right]}, \tag{42}$$

provided that $S_F[c_{0b} \frac{\dot{x}_{1r}}{S_L} + k_{0b} \frac{x_{1r}}{S_L} + \alpha_b z] \neq 0$, otherwise $u = 0$. $S_F$ is the damper force scaling factor and $S_L$ is the piston displacement scaling factor, as discussed in section 'MR Damper'. Due to measurements of the accelerometers and the accurate fitting of the Bouc–Wen model for the MR damper, all state variables in Equation (42) were also available for feedback. Therefore, controller Equation (42) could be implemented.

The stability of the controller of Equation (42) can be proved in a similar way to that of Equation (35). Consider again the backstepping variables of Equation (36) and the Lyapunov function candidate and its derivative of Equations (37) and (38). Substitution of Equations (11), (33)–(36), and (42) into Equation (38) also yields $\dot{V} = -h_1 e_1^2 - h_2 e_2^2 < 0$, which guarantees the stability of the system.

## EXPERIMENTAL RESULTS

The backstepping controllers were tested in the RTHT setup described previously. The numerical model, i.e., the three-story building and the controller, were implemented in MATLAB/Simulink. The ordinary differential equation solver used is the fourth-order Runge–Kutta method with a time step $T_s = 5 \times 10^{-4}$ s. The structure was subject to three different earthquake records, namely El Centro, Loma Prieta, and Northridge, as shown in Figure 13; the scale amplitude used was 0.4. The controllers were implemented with $h_1 = 1 \times 10^{-3}$ and $h_2 = 1 \times 10^{-6}$.

The experiments were performed in five different scenarios: no damper in the structure (uncontrolled); damper in passive mode OFF, i.e., no current flow in the damper coils (0 V); damper in passive mode ON, i.e., the maximum current allowed flows through the damper coils (5 V); model-based backstepping controller ON (Mod. based BS.); and finally, backstepping control based on the modified version of the clipped optimal algorithm (Clipped BS.). In order to evaluate the performance of the damper in all cases, the peak displacements and accelerations and the root mean square (RMS) displacements and accelerations of each floor were analyzed. In addition, the performance indices of

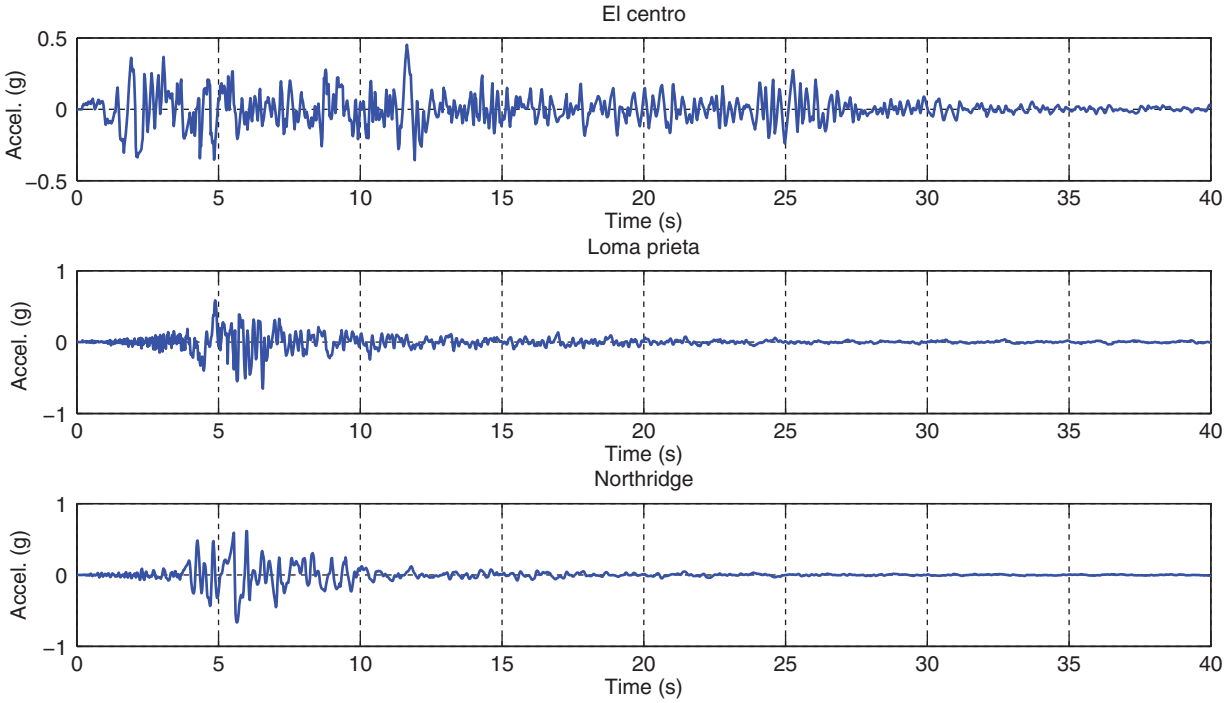


***Figure 13.*** *Records of El Centro, Loma Prieta, and Northridge earthquakes.*

***Table 1. Performance indices.***

| Index | Description |
|---|---|
| $J_1 = \max_{i,t}\left(\frac{\lvert\ddot{x}_{ai,c}(t)\rvert}{\ddot{x}^{\max}_{a,u}(t)}\right)$ | Normalized peak floor acceleration. |
| $J_2 = \max_{i,t}\left(\frac{\lVert\ddot{x}_{ai,c}(t)\rVert}{\lVert\ddot{x}^{\max}_{a,u}\rVert}\right)$ | Normed peak acceleration |
| $J_3 = \max(\lvert x_{2r}(t) - x_{1r}(t)\rvert)$ | Interstory drift between 2nd and 1st floor. |
| $J_4 = \max(\lvert x_{3r}(t) - x_{2r}(t)\rvert)$ | Interstory drift between 3rd and 2nd floor. |
| $J_5 = \max_{t,i}\left(\frac{\lvert f_{mrd}(t)\rvert}{W}\right)$ | Maximum control force. |
| $J_6 = \left(\frac{1}{\tau}\int_0^{\tau}[\dot{x}_m(t)]^2 dt\right)^{1/2}$ | RMS control power. |

Table 1 were used in performance evaluation. $J_1$ is the maximum floor acceleration in the controlled case, normalized by the maximum floor acceleration of the structure in the uncontrolled case. The index $J_2$ considers the norm of the acceleration in a manner similar to $J_1$; $J_3$ and $J_4$ measure the peak inter-story drift between the 2nd and 1st floors and between the 3rd and 2nd floors, respectively, and $J_5$ is the ratio between the peak control force and the weight of the whole structure. Finally, $J_6$ measures the RMS control effort damper.

Table 2 shows the peak and RMS values of displacement and acceleration of the structure when subject to the seismic motions and in each of the cases described earlier. It can be noted that both backstepping controllers are able to reduce the displacement and acceleration response compared with the uncontrolled case. This is also true for the passive OFF case. In fact, when no current flowed through the damper, no major differences were observed compared with the uncontrolled case. For instance, the difference in the third-floor peak and RMS acceleration between the uncontrolled and passive OFF cases when the structure was subject to the El Centro earthquake was 11.97% and 31.38%, respectively. For comparison, these differences significantly increased to 52.44% and 71.89%, respectively, when comparing the uncontrolled and the backstepping control cases.

On the other hand, results of the passive ON cases show different performances. It could be noted that the reduction of peak and RMS displacements achieved in the passive ON cases was greater than that achieved by the backstepping controllers. However, the reduction in peak and RMS accelerations achieved by the controllers was in general greater than that achieved in passive ON cases. For example, the differences between the third-floor peak and RMS accelerations of the structure when subject to the El Centro earthquake were 18.37%

*Table 2. Peak and RMS responses under El Centro, Loma Prieta, and Northridge earthquakes.*

| Measure | Uncont. | Pas. OFF | Pas. ON | Clipped BS. | Mod. BS. |
|---|---|---|---|---|---|
| **El Centro** | | | | | |
| Peak $x_{1r}$ (cm) | 7.26 | 5.78 | 1.85 | 3.11 | 3.20 |
| Peak $x_{2r}$ (cm) | 11.23 | 9.09 | 3.48 | 4.75 | 4.63 |
| Peak $x_{3r}$ (cm) | 13.37 | 10.95 | 4.69 | 5.86 | 5.47 |
| Peak $\ddot{x}_{1r}$ (m/s$^2$) | 4.51 | 3.42 | 2.74 | 3.40 | 3.06 |
| Peak $\ddot{x}_{2r}$ (m/s$^2$) | 5.67 | 4.66 | 3.07 | 3.40 | 2.70 |
| Peak $\ddot{x}_{3r}$ (m/s$^2$) | 6.35 | 5.59 | 3.70 | 3.47 | 3.02 |
| RMS $x_{1r}$ (cm) | 2.97 | 2.02 | 0.37 | 0.59 | 0.81 |
| RMS $x_{2r}$ (cm) | 4.71 | 3.21 | 0.78 | 0.97 | 1.28 |
| RMS $x_{3r}$ (cm) | 5.67 | 3.86 | 1.05 | 1.21 | 1.55 |
| RMS $\ddot{x}_{1r}$ (m/s$^2$) | 1.54 | 1.09 | 0.76 | 0.73 | 0.54 |
| RMS $\ddot{x}_{2r}$ (m/s$^2$) | 2.25 | 1.54 | 0.71 | 0.67 | 0.68 |
| RMS $\ddot{x}_{3r}$ (m/s$^2$) | 2.74 | 1.88 | 0.88 | 0.77 | 0.83 |
| **Loma Prieta** | | | | | |
| Peak $x_{1r}$ (cm) | 4.69 | 3.73 | 1.90 | 3.19 | 3.21 |
| Peak $x_{2r}$ (cm) | 7.39 | 6.28 | 3.58 | 5.09 | 5.17 |
| Peak $x_{3r}$ (cm) | 8.88 | 8.05 | 4.45 | 6.34 | 6.25 |
| Peak $\ddot{x}_{1r}$ (m/s$^2$) | 5.16 | 4.21 | 3.53 | 3.27 | 2.34 |
| Peak $\ddot{x}_{2r}$ (m/s$^2$) | 3.92 | 3.19 | 3.50 | 2.82 | 2.62 |
| Peak $\ddot{x}_{3r}$ (m/s$^2$) | 6.28 | 5.71 | 3.32 | 3.60 | 3.04 |
| RMS $x_{1r}$ (cm) | 2.39 | 1.39 | 0.34 | 0.50 | 0.59 |
| RMS $x_{2r}$ (cm) | 3.77 | 2.18 | 0.64 | 0.81 | 0.92 |
| RMS $x_{3r}$ (cm) | 4.54 | 2.63 | 0.84 | 0.99 | 1.11 |
| RMS $\ddot{x}_{1r}$ (m/s$^2$) | 1.50 | 0.93 | 0.69 | 0.58 | 0.41 |
| RMS $\ddot{x}_{2r}$ (m/s$^2$) | 1.84 | 1.09 | 0.61 | 0.55 | 0.50 |
| RMS $\ddot{x}_{3r}$ (m/s$^2$) | 2.27 | 1.34 | 0.67 | 0.60 | 0.59 |
| **Northridge** | | | | | |
| Peak $x_{1r}$ (cm) | 6.77 | 6.56 | 3.63 | 4.61 | 5.81 |
| Peak $x_{2r}$ (cm) | 10.18 | 9.97 | 6.05 | 7.85 | 9.33 |
| Peak $x_{3r}$ (cm) | 11.97 | 11.64 | 6.94 | 9.17 | 10.95 |
| Peak $\ddot{x}_{1r}$ (m/s$^2$) | 5.81 | 4.80 | 2.83 | 4.51 | 3.29 |
| Peak $\ddot{x}_{2r}$ (m/s$^2$) | 6.15 | 5.85 | 4.61 | 5.88 | 5.70 |
| Peak $\ddot{x}_{3r}$ (m/s$^2$) | 8.21 | 7.21 | 4.79 | 5.67 | 6.14 |
| RMS $x_{1r}$ (cm) | 2.17 | 1.37 | 0.40 | 0.57 | 0.76 |
| RMS $x_{2r}$ (cm) | 3.41 | 2.16 | 0.71 | 0.94 | 1.17 |
| RMS $x_{3r}$ (cm) | 4.11 | 2.60 | 0.93 | 1.15 | 1.41 |
| RMS $\ddot{x}_{1r}$ (m/s$^2$) | 1.55 | 0.94 | 0.63 | 0.67 | 0.58 |
| RMS $\ddot{x}_{2r}$ (m/s$^2$) | 1.67 | 1.05 | 0.61 | 0.65 | 0.66 |
| RMS $\ddot{x}_{3r}$ (m/s$^2$) | 1.34 | 2.16 | 0.72 | 0.74 | 0.79 |

and 12.5%, respectively. When the structure was subject to the Loma Prieta earthquake, these values were 8.4% and 13.55%, respectively; finally, in the Northridge earthquake case, these differences were 28.18% and 9.72%, respectively. In this last case, a higher reduction was achieved by the passive ON damper.

The performance indices for the different seismic excitations are shown in Table 3. Performance indices $J_1$–$J_4$ showed that both backstepping controllers had a similar performance. This also confirmed the results of Table 2, which show a reduction in acceleration and displacement response when compared with the uncontrolled and passive OFF cases. It also shows that the controllers have a similar performance to the passive ON case, achieving in general a greater reduction in acceleration, as discussed earlier.

An important result that can be found in Table 3 is that of indices $J_5$ and $J_6$. These indices showed that the control effort in the case of the controller based on the modified clipped optimal algorithm was larger than that of the controller based on the dynamics of the MR damper. This could be explained by the fact that in the first case, the voltage switched between two extreme cases (no current flowing through the damper coil and maximum current flowing through the damper coil). In the second case, the control signal changed in a smoother fashion and in turn, the control effort was reduced. Furthermore, the reduction in RMS control

***Table 3. Controller performance indices under El Centro, Loma Prieta, and Northridge earthquakes.***

| Earthquake | Controller | $J_1$ | $J_2$ | $J_3$ (cm) | $J_4$ (cm) | $J_5$ | $J_6$ (N) |
|---|---|---|---|---|---|---|---|
| **El Centro** | Uncontrolled | – | – | 4.06 | 2.27 | – | – |
| | Passive OFF | 0.58 | 0.32 | 3.44 | 2.00 | 0.09 | 44.43 |
| | Passive ON | 0.58 | 0.32 | 1.93 | 1.32 | 0.13 | 420.66 |
| | Clipped BS. | 0.55 | 0.28 | 1.75 | 1.24 | 0.12 | 338.71 |
| | Mod. based BS. | 0.48 | 0.31 | 1.72 | 1.08 | 0.08 | 253.42 |
| **Loma Prieta** | Uncontrolled | – | – | 2.75 | 2.24 | – | – |
| | Passive OFF | 0.91 | 0.59 | 2.60 | 2.04 | 0.01 | 42.91 |
| | Passive ON | 0.56 | 0.30 | 1.71 | 1.19 | 0.12 | 351.00 |
| | Clipped BS. | 0.58 | 0.34 | 1.93 | 1.29 | 0.12 | 288.58 |
| | Mod. based BS. | 0.48 | 0.34 | 2.01 | 1.09 | 0.09 | 227.54 |
| **Northridge** | Uncontrolled | – | – | 3.89 | 2.93 | – | – |
| | Passive OFF | 0.88 | 0.62 | 3.70 | 2.58 | 0.09 | 36.25 |
| | Passive ON | 0.58 | 0.33 | 2.62 | 1.71 | 0.12 | 326.37 |
| | Clipped BS. | 0.72 | 0.38 | 3.49 | 2.03 | 0.12 | 286.87 |
| | Mod. based BS. | 0.75 | 0.41 | 2.20 | 2.03 | 0.11 | 231.07 |

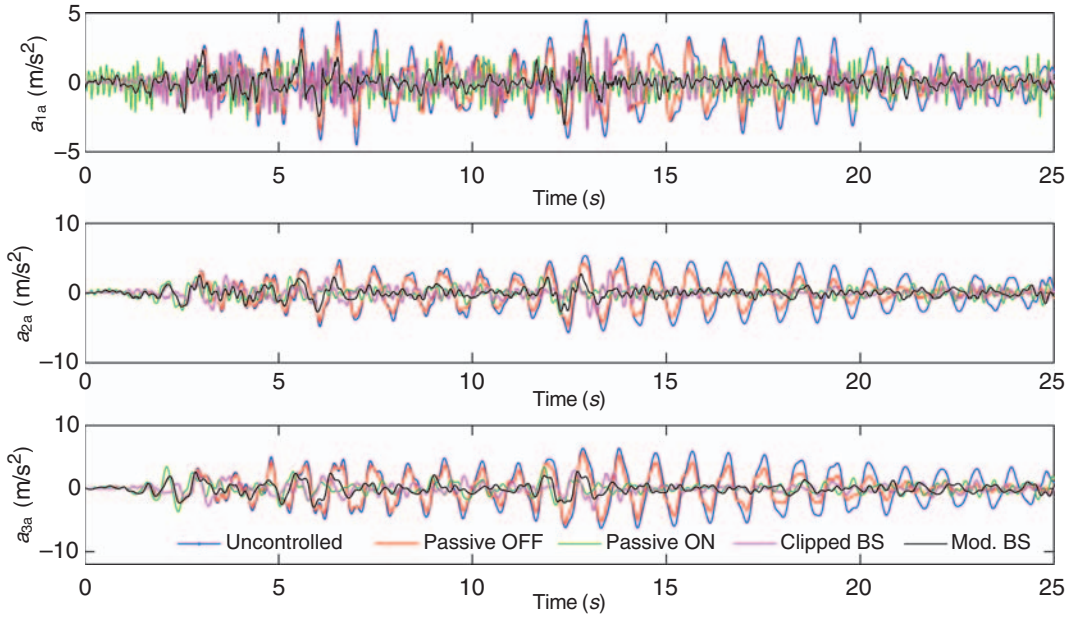


***Figure 14.*** *Structure acceleration response under the El Centro earthquake.*

effort ($J_6$) achieved by the model-based backstepping controller compared with the passive ON case was 39.86% (El Centro), 35.17% (Loma Prieta), and 29.20% (Northridge).

Figures 14–19 graphically depict some of the tabular results. Figures 14 and 15 show the acceleration and displacement response of each floor when the structure was subject to the El Centro earthquake. All the cases studied were mutually compared, i.e., the uncontrolled, passive and control cases. It could be observed from these figures that the passive OFF damper did not improve the structure response in a significant way, as can be seen in Tables 2 and 3. The first-floor acceleration and displacement under the three earthquakes are depicted in Figures 16 and 17, respectively. The uncontrolled, passive ON and model-based backstepping control cases are shown. It could be observed that the acceleration response was significantly improved by the backstepping controller, as discussed earlier. It could also be noted that the displacement response of the passive ON damper and that of the controller were similar. Finally, Figures 18 and 19 show the performance of the MR damper (the actual damper, i.e., not scaled) and in particular, a comparison of the dynamics

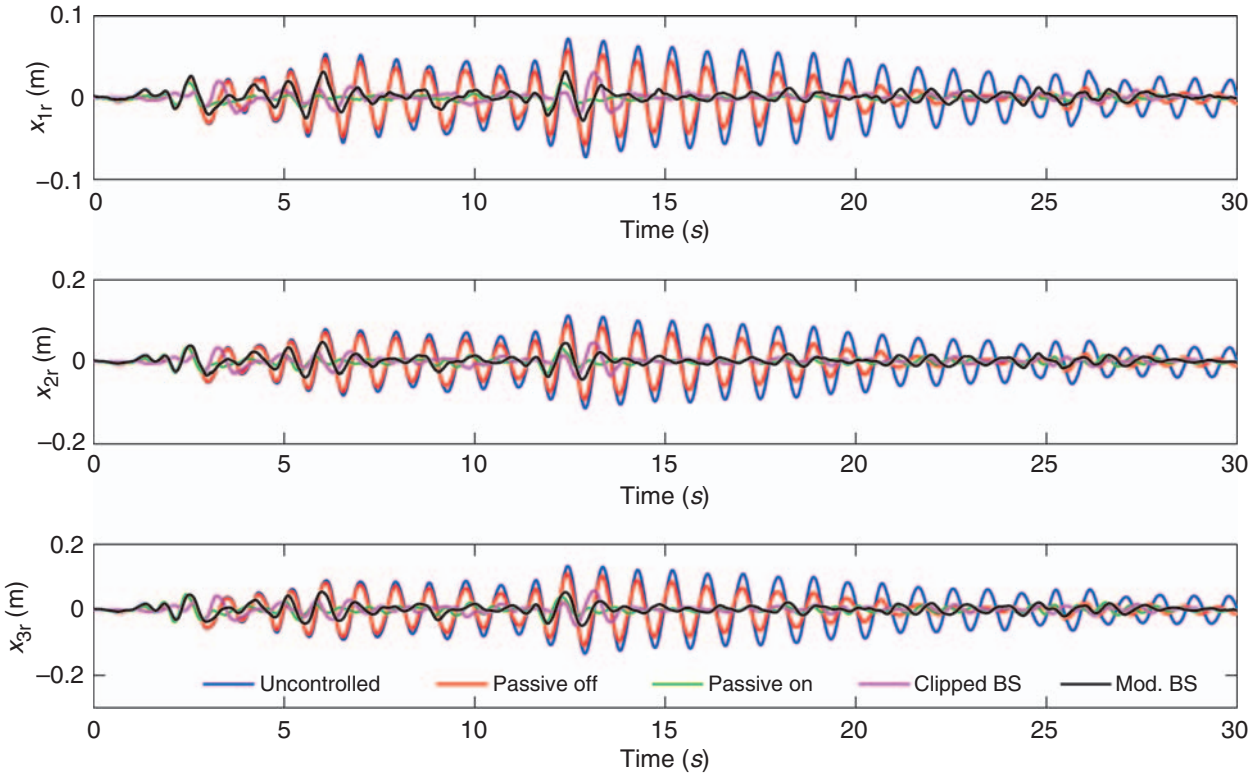


***Figure 15.*** *Structure displacement response under the El Centro earthquake.*

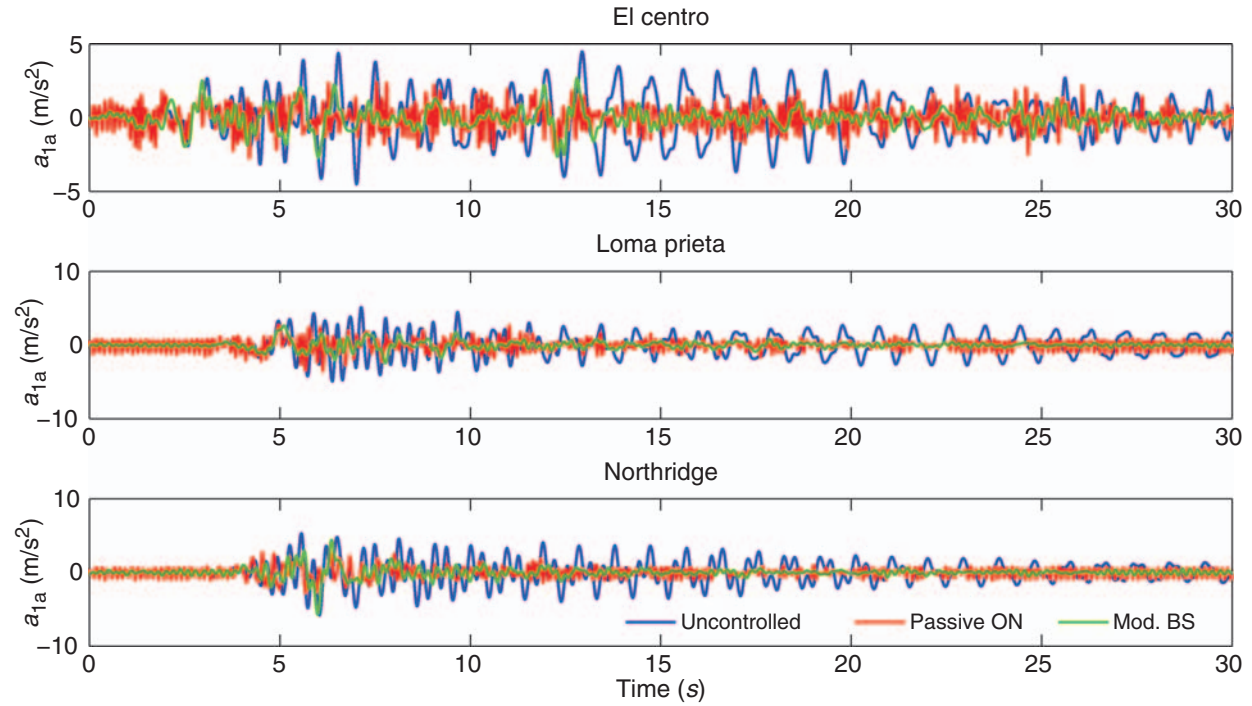


***Figure 16.*** *First floor acceleration response to El Centro, Loma Prieta, and Northridge earthquakes.*

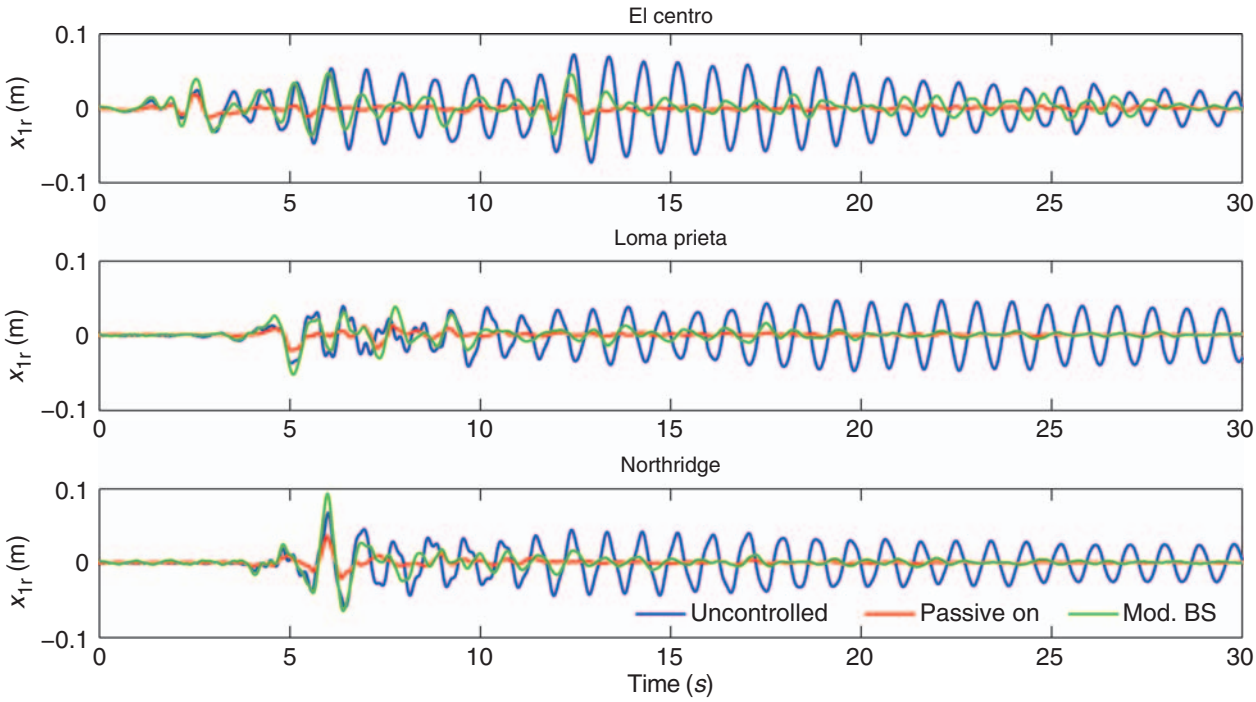


***Figure 17.*** *First floor displacement response to El Centro, Loma Prieta, and Northridge earthquakes.*

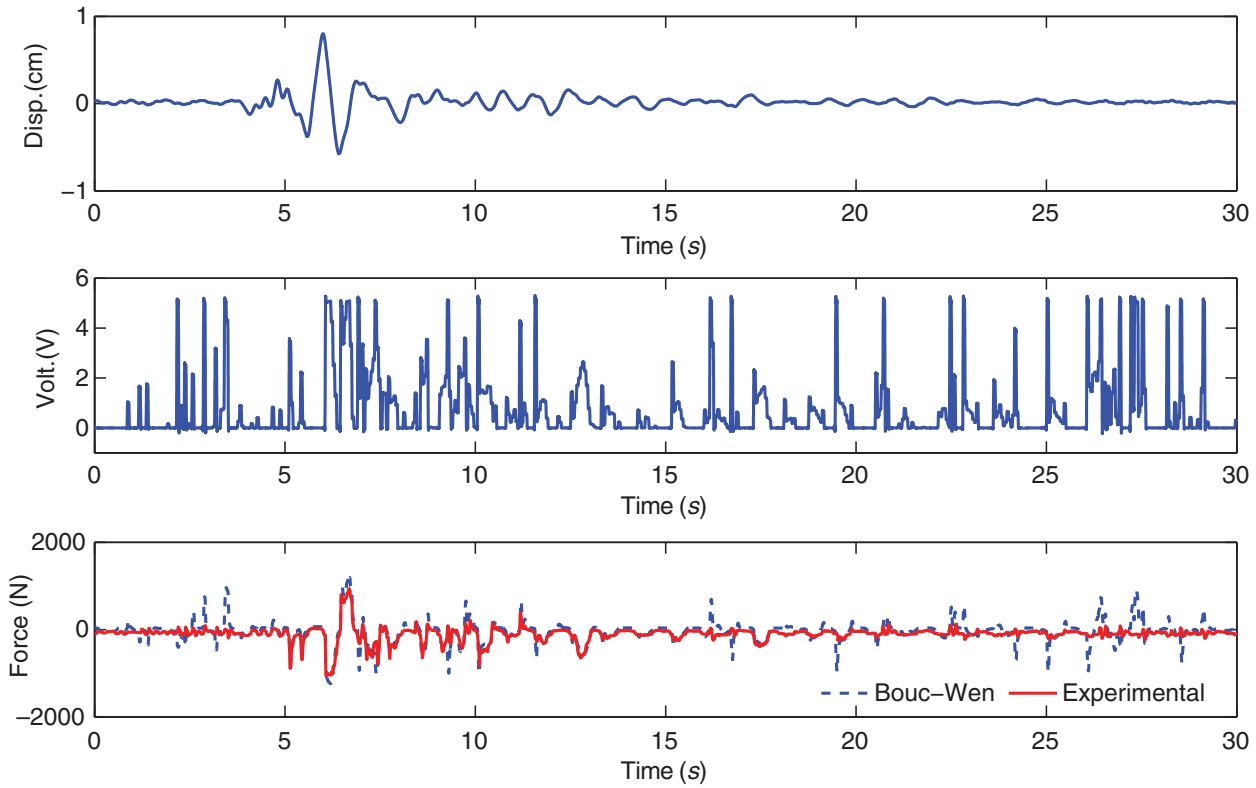


***Figure 18.*** *Model-based Backstepping: MR damper response under Northridge earthquake.*

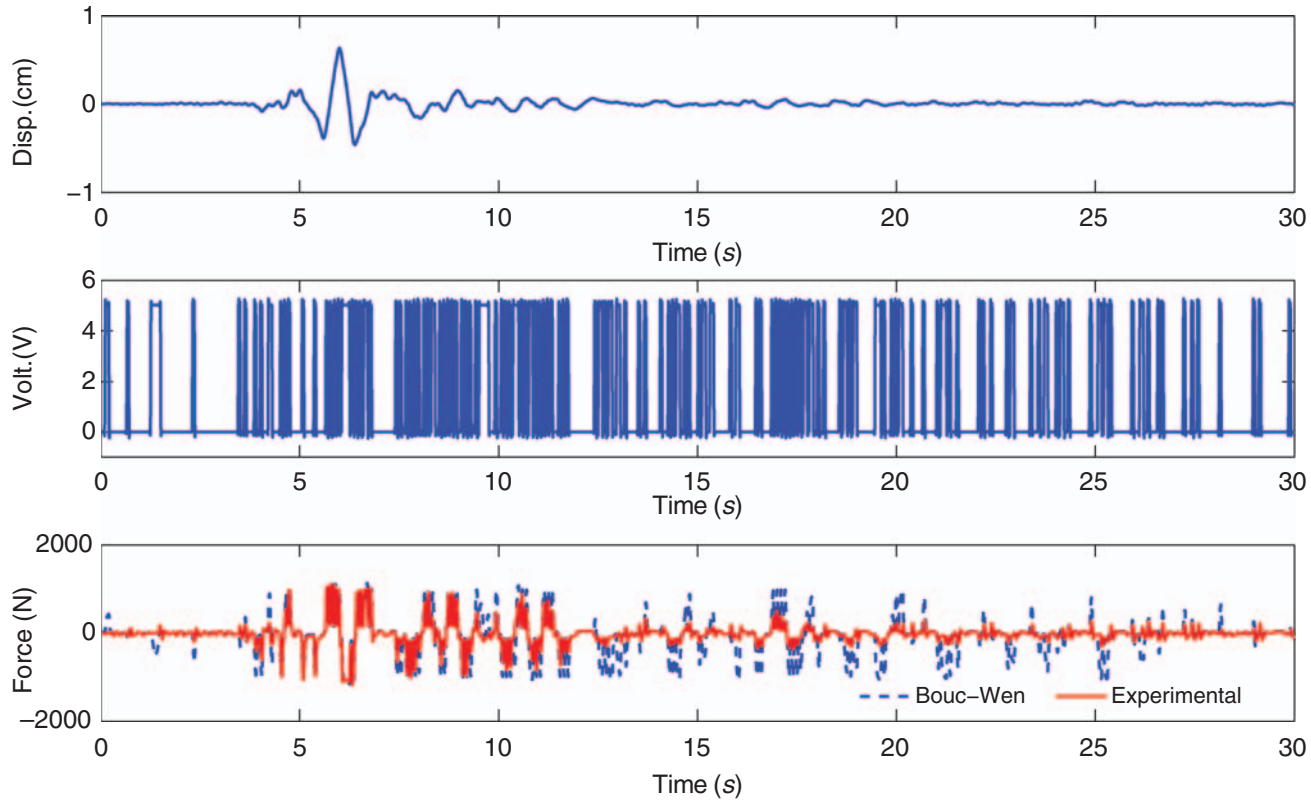


***Figure 19.*** *Clipped Backstepping: MR damper response under Northridge earthquake.*

predicted by the Bouc–Wen model and that obtained experimentally when subject to the Northridge earthquake.

## CONCLUSIONS

In this article, a new semiactive controller based on the backstepping technique has been proposed for reducing the vibrations in a three-story building equipped with an MR damper. Two variations were presented: one based on a modification of the clipped optimal algorithm and another based on the non-linear dynamics of the MR damper. The controllers were experimentally tested in a RTHT setup. Both controllers successfully achieved the proposed goal of reducing the structure response when subject to seismic motion. Furthermore, the backstepping controllers significantly improved the acceleration response of the structure when compared with a passive damper operating at the maximum power allowed. This could be achieved with a reduction in the control effort, despite the degradation of the displacement response. Moreover, the backstepping controller based on the damper dynamics showed the best performance in reducing acceleration and control effort.

## ACKNOWLEDGMENTS

This work has been partially funded by the European Union (European Regional Development Fund) and the Commission of Science and Technology of Spain (CICYT) through the coordinated research projects DPI-2005-08668-C03 and by the government of Catalonia through SGR00296. M. Zapateiro acknowledges the FI and BE Grants of the Department for Innovation, University and Enterprise of the Government of Catalonia (Spain). B.M. Phillips is supported under a National Science Foundation Graduate Research Fellowship.

## REFERENCES

Carrion, J. and Spencer, B. 2007. Model-based Strategies for Real-time Hybrid Testing, Technical Report, University of Illinois at Urbana, Champaign.

Dyke, S.J., Spencer Jr, B.F., Sain, M.K. and Carlson, J.D. 1998. "An Experimental Study of MR Dampers for Seismic Protection," *Smart Materials and Structures*, 7:693–703.

Dyke, S., Spencer, B., Sain, M. and Carlson, J. 1996. "Modeling and Control of Magnetorheological Dampers for Seismic Response Reduction," *Smart Materials and Structures*, 5:565–575.

Jansen, L. and Dyke, S. 2000. "Semiactive Control Strategies for MR Dampers: Comparative Study," *Journal of Engineering Mechanics*, 126:795–803.

Karimi, H.R., Zapateiro, M. and Luo, N. 2009. "Wavelet-based Parameter Identification of a Nonlinear Magnetorheological Damper," *International Journal of Wavelets, Multiresolution and Image Procesing*, 7, In press.

Kim, H. and Roschke, P. 2006. "Fuzzy Control of Base-isolation System Using Multiobjective Genetic Algorithm," *Computer-Aided Civil and Infrastructure Engineering*, 21:436–446.

Krstic, M., Kanellakopoulos, I. and Kokotovic, O. 1995. *Nonlinear and Adaptive Control Design*, John Wiley and Sons.

Luo, N., Rodellar, J., la Sen, M.D. and Vehí, J. 2000. "Output Feedback Sliding Mode Control of Base Isolated Structures," *Journal of the Franklin Institute*, 337:555–577.

Luo, N., Rodellar, J. and Villamizar, R. 2003. "Robust Control Law for a Friction-based Semiactive Controller of a Two-span Bridge," In: *Proceeding of the SPIE 10th Annual International Symposium on Smart Structures and Materials*, San Diego, California, USA.

Luo, N., Villamizar, R. and Vehi, J. 2007. "Backstepping Control of Nonlinear Building Structures with Hysteretic and Frictional Dynamics," In: *European Control Conference*, Kos, Greece.

McClamroch, N. and Gavin, H. 1995. "Closed Loop Structural Control Using Electrorheological Dampers," In: *Proceedings of the American Control Conference*, Seattle, Washington, USA.

McClamroch, N., Gavin, H., Ortiz, D. and Hanson, R. 1994. "Electrorheological Dampers and Semi-active Structural Control," In: *Proceedings of the 33rd Conference on Decision and Control,* Lake Buena Vista, Florida.

Moon, S., Bergman, L. and Voulgaris, P. 2003. "Sliding Mode Control of Cable-stayed Bridge Subjected to Seismic Excitation," *Journal of Engineering Mechanics*, 129:71–78.

Nagarajaiah, S., Narasimhan, S., Agrawal, A. and Tang, P. 2006. "Semiactive Lyapunov Controller for Phase II Seismic Isolated Bridge Benchmark," In: *Structures Congress 2006*, St. Louis, Missouri, USA.

Park, C. and Jeon, D. 2002. "Semiactive Vibration Control of a Smart Seat with an MR Fluid Damper Considering its Time Delay," *Journal of Intelligent Material Systems and Structures*, 13:521–524.

Schurter, K. and Roschke, P. 2001. "Neuro-fuzzy Control of Structures Using Acceleration Feedback," *Smart Materials and Structures*, 10:770–779.

Spencer, B., Dyke, S., Sain, M. and Carlson, J. 1997. "Phenomenological Model of a Magnetorheological Damper," *ASCE Journal of Engineering Mechanics*, 123:230–238.

Spencer, B. and Sain, M. 1997. "Controlling Buildings: a New Frontier in Feedback," *IEEE Control Systems Magazine*, 17:19–35.

Spencer, B. and Song, T. 1999. "New Applications and Development of Active, Semi-active and Hybrid Control Techniques for Seismic and Non-seismic Vibration in the USA," In: *Proceedings of International Post-SMIRT Conference Seminar on Seismic Isolation, Passive Energy Dissipation and Active Control of Vibration of Structures*, Cheju, Korea.

Villamizar, R., Luo, N., Dyke, S. and Vehi, J. 2005. "Experimental Verification of Backstepping Controllers for Magnetorheological MR Dampers in Structural Control," In: *Proceedings of the 13th Mediterranean Conference on Control and Automation,* Limassol, Cyprus.

Villamizar, R., Luo, N., Vehi, J. and Rodellar, J. 2003. "Semiactive Sliding Mode Control of Uncertain Base Isolated Structures with Actuator Dynamics," In: *Proceeding SPIE 10th Annual International Symposium on Smart Structures and Materials*, Warsaw, Poland.

Villamizar, R., Luo, N., Vehi, J. and Rodellar, J. 2004. "Active and Semiactive qft Control for the Structural Vibration Attenuation," In: *MOVIC – Conference on Mechanical Vibration and Noise*, St. Louis, USA.

Wang, X. and Gordaninejad, F. 2002. "Lyapunov-based Control of a Bridge Using Magnetorheological Fluid Dampers," *Journal of Intelligent Material Systems and Structures*, 13:415–419.

Yang, G., Spencer, B., Carlson, J. and Sain, M. 2002. "Large-scale MR Fluid Dampers: Modeling and Dynamic Performance Considerations," *Engineering Structures*, 24:309–323.

Yoshioka, H., Ramallo, J. and Spencer, B. 2002. "'Smart' Based Isolation Strategies Employing Magnetorheological Dampers," *Journal of engineering mechanics*, 128:540–551.

Zapateiro, M., Luo, N. and Karimi, H.R. 2008. "QFT Control for Vibration Reduction in Structures Equipped with MR Dampers," In: *American Control Conference*, Seattle, USA.